



This is a repository copy of *Effects of the granule composition on the compaction behavior of deformable dry granules*.

White Rose Research Online URL for this paper:
<http://eprints.whiterose.ac.uk/119748/>

Version: Submitted Version

Article:

Mitra, B., Hilden, J. and Litster, J.D. orcid.org/0000-0003-4614-3501 (2016) Effects of the granule composition on the compaction behavior of deformable dry granules. *Powder Technology*, 291. pp. 487-498. ISSN 0032-5910

<https://doi.org/10.1016/j.powtec.2016.01.009>

Reuse

This article is distributed under the terms of the Creative Commons Attribution-NonCommercial-NoDerivs (CC BY-NC-ND) licence. This licence only allows you to download this work and share it with others as long as you credit the authors, but you can't change the article in any way or use it commercially. More information and the full terms of the licence here: <https://creativecommons.org/licenses/>

Takedown

If you consider content in White Rose Research Online to be in breach of UK law, please notify us by emailing eprints@whiterose.ac.uk including the URL of the record and the reason for the withdrawal request.



eprints@whiterose.ac.uk
<https://eprints.whiterose.ac.uk/>

Effect of the granule composition on the compaction behavior of deformable dry granules

Biplob Mitra^{1,2}, Jon Hilden^{2,3}, James D Litster^{1,4}

¹Department of Industrial and Physical Pharmacy, Purdue University, West Lafayette, IN, USA

²Small Molecule Design and Development, Eli Lilly and Co., Indianapolis, IN, USA

³School of Materials Engineering, Purdue University, West Lafayette, IN, USA

⁴School of Chemical Engineering, Purdue University, West Lafayette, IN, USA

ABSTRACT:

Calibration of the Drucker Prager Cap (DPC) model parameters provides a means for a deeper understanding of the impact of granule composition on the compaction properties of dry granules independent of their solid fraction (SF). In this study, monodisperse granules of mixtures of microcrystalline cellulose and mannitol (0%, 25%, 50%, 75% and 100% mannitol) prepared as small cylindrical compacts with well-defined size, shape and SF (0.58) were used as model dry granules. DPC parameters--namely, cohesion, internal friction angle, cap eccentricity, and hydrostatic yield strength of materials--were determined from the diametrical and uniaxial compression, and in-die compaction tests. Elastic properties such as Young's modulus and Poisson's ratios were also determined from the in-die compaction test. Higher level of MNT in granules required a lower compression pressure to obtain a low SF tablet but higher compression pressure to obtain a high SF tablets. Properties such as cohesion and diametrical tensile strength go through a maximum as the mannitol level increases in the binary granules, and clearly do not follow the linear mixing rule. At an industrially-relevant tablet solid fraction of 0.88, granules with 75% mannitol exhibited the highest cohesion, and produced the strongest tablet. Other properties either approximately follow the linear mixing rule (e.g., hydrostatic yield strength, young's modulus and Poisson's ratio) where some interactions between the constituents are present, or not sensitive to the composition (e.g., internal angle of friction). In general, the compaction behavior of granules of a multicomponent system may not be precisely estimated from the properties of individual components, simply by using the linear mixing rule.

KEYWORDS: Dry Granules, Powder Mixture, Tablet, Solid Fraction, Tensile Strength, Drucker-Prager Cap (DPC) Model

Correspondence to:

Prof. James D Litster

Purdue University

480 Stadium Mall Drive, Room 027A

West Lafayette, IN 47907, USA

Telephone +1 765 496 2836

Fax +1 765 494 0805

Email address: jlitster@purdue.edu

1. Introduction

Most pharmaceutical tablets are manufactured from a homogeneous blend of powders of varying physical, mechanical, and functional properties. The mechanical properties of a formulation are typically balanced by using a combination of plastically deformable excipients such as microcrystalline cellulose (MCC), pregelatinized starch, cellulose, polyethylene glycol (PEG) and brittle excipients such as dicalcium phosphate, lactose, and mannitol. In general, a granulation step is involved, where larger multi-particulate entities of drug and excipient mix are produced [1]. Granulation locks the powder blend homogeneity, ensures robust downstream processing of the formulation to produce tablets with desired physico-mechanical properties (e.g., SF, strength, friability) and critical quality attributes (content uniformity and dissolution). Granules that are composed of appropriate ingredients, at an appropriate ratio, with appropriate properties, are important for robust production of quality tablets.

In our previous study, we have demonstrated that SF of dry granules of a single component (MCC) significantly impacts the tablet fracture and tensile strength [2,3]. By calibrating the Drucker Prager Cap (DPC) model parameters we have also showed that MCC granule SF does not affect the plastic strain driven densification in a confined compression process but increases the propensity to fail [4]. In a multicomponent system, the compaction behaviour of one component is expected to interact with that of the other components, and alter the granule and tablet properties. In the literature [5,6,7,8,9,10] the effect of an individual component on the compaction behavior of other components in the granule has not been studied with adequate separation from the effect of granule physical and mechanical properties. To mechanistically understand this, granule composition and granule properties need to be precisely controlled and independently varied. This study presents calibration of the DPC parameters using simple systems that allow analysis of effects of the levels of mannitol on the compaction behavior of MCC/mannitol binary granules without any interference from the granule SF. In addition, elastic properties such as Poisson's ratio and Young's modulus of the granules are presented.

2. DPC Model

The DPC model illustrates the permanent deformation of materials as a function of SF of the tablet in the hydrostatic stress-effective stress (p - q) plane. p causes volumetric changes and q causes shear-based distortion without volume change. For a given yield envelope such as that shown in Figure 1, application of stress states within the envelope produce only elastic distortions. Stress states exceeding the yield envelope produce permanent deformation. The deformation involves fracture if the linear portion of the envelope is exceeded, but involves further densification of the powder if the elliptical cap portion is exceeded. During consolidation, the yield envelope expands as the solid fraction increases and gives a series of yield surfaces which describes the complete behavior of a material. Four independent yield surface parameters required for complete calibration of the model are cohesion (d), internal angle of friction (β), cap eccentricity parameter (R) and hydrostatic yield stress (p_b). Detailed description of the model is available in the literature [11].

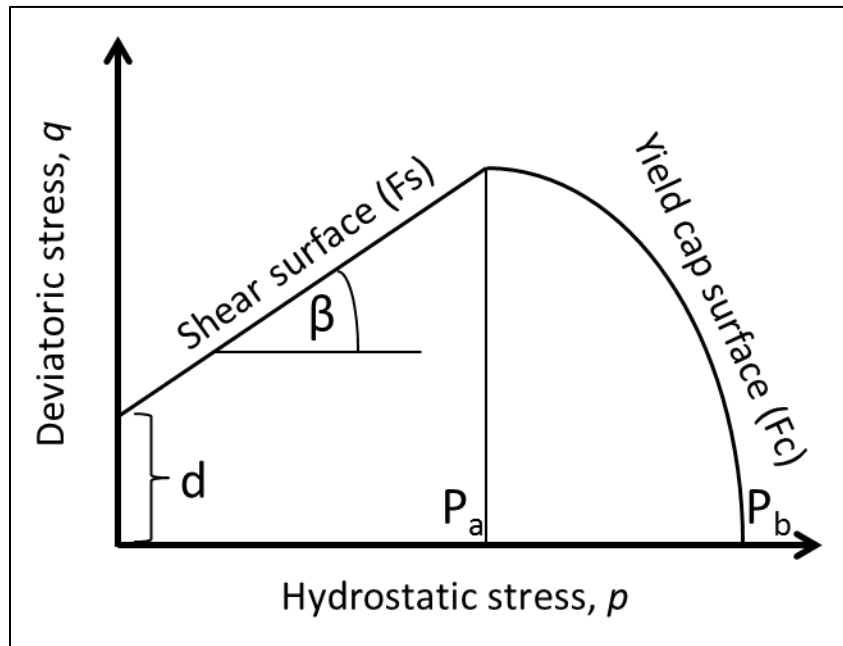


Figure 1. 2D Yield Surface for the Drucker Prager Cap Model [4]

3. Materials and Methods

3.1 Virgin MCC and MNT Powders

MCC (Avicel PH200, FMC, PA, USA) and MNT (Pearlitol SD200, Roquette, IL, USA) were used as starting materials to produce dry granules that were forward processed into tablets. The spray dried MCC particles have fibrous morphology with very high surface area, composed of millions of microfibrils that are 70% crystalline and 30% amorphous (Figure 2A) [12].

MCC structure deforms plastically under compression pressure. On the other hand, spray dried MNT particles are porous, relatively fragile agglomerates of small MNT crystals (Figure 2B) [13]. Therefore, it is reasonable to expect that the spray dried MNT particles undergo a two stage deformation process—first, the secondary agglomerates would fracture under low pressure, and subsequently, the MNT crystals would fracture under high pressure.

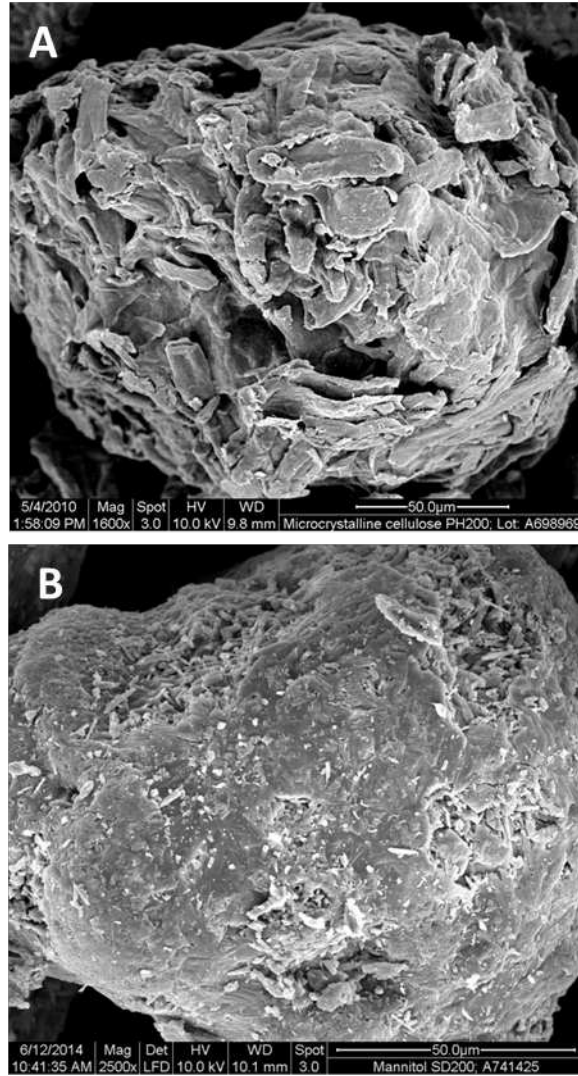


Figure 2. SEM Image of MCC (A) and MNT Particle (B)

A 150 to 250 μm size fraction of MCC and MNT powders were obtained by sieving and were referred to as 200 μm V-MCC and 200 μm V-MNT, respectively. Both powders were equilibrated at 20°C/30% RH condition for 24 hours prior to forward processing to eliminate the impact of moisture content variability on compact's mechanical properties [14]. The true density of V-MCC and V-MNT are 1.556 g/cc [2] and 1.514 g/cc [15]. Solid fraction of the tapped powder bed was 0.25 and 0.48 for V-MCC and V-MNT, respectively. Figure 3 illustrates the study design.

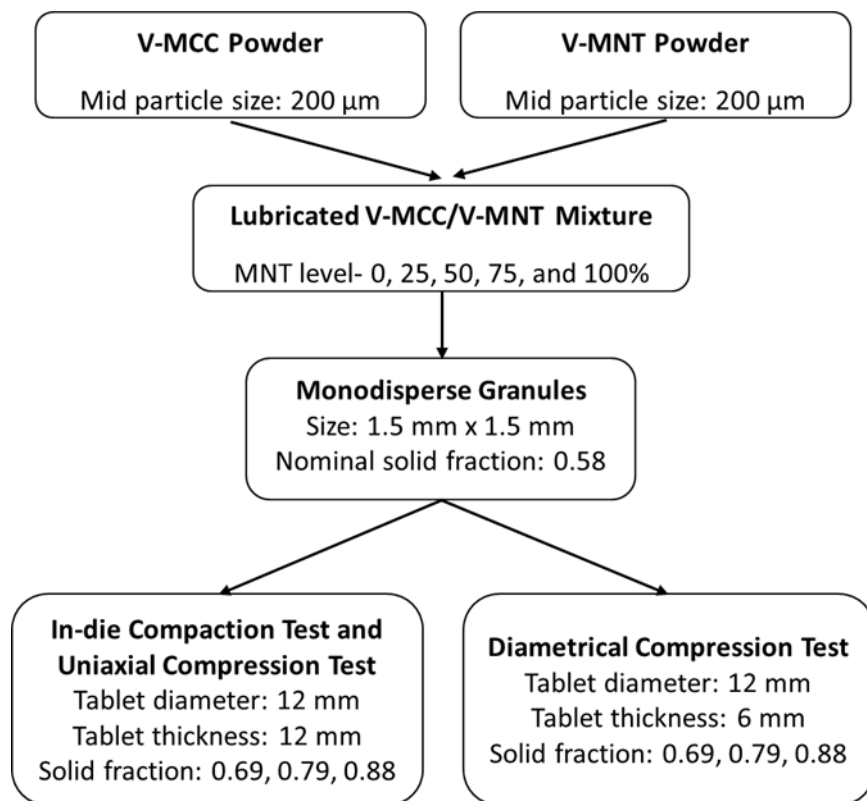


Figure 3. Schematic Diagram of the Study Design

3.2 Monodisperse Granule Preparation

V-MCC and V-MNT powders were mixed together for 10 minutes using a Turbula mixer (model T2F, Willy A. Bachofen AG, Basel, Switzerland) at 32 rpm to produce powder blends containing 25, 50, and 75% Mannitol. Individual powders and their binary mixtures were then mixed for 20 minutes with 1% sodium stearyl fumarate as a lubricant. Monodisperse granules of precisely controlled size (1.5 mm diameter x 1.5 mm thickness), shape (biconvex cylindrical compact), and SF (0.58 ± 0.01) were produced by directly compressing the powder on a Korsch EK0 (Korsch Pressen, Berlin, Germany) tablet press equipped with standard concave, multi-tip tooling. Monodisperse granules were equilibrated at 20°C/30% RH condition for at least 24 hours and stored in an airtight glass container to allow for any viscoelastic recovery prior to characterizing for size and SF and forward processing into tablets.

3.3 Compression of Tablets

For each powder blend composition, 5 tablets were produced at each of 3 different solid fractions (0.69, 0.79, and 0.88) and two different thicknesses (6 mm and 12 mm) for a total of 30 tablets per blend. Tablets were produced using an Instron universal testing machine (model 5569, Instron Ltd., Buckinghamshire, United Kingdom) equipped with 12 mm flat face tooling. Before compacting each tablet, the die wall and punch faces were lubricated with magnesium stearate powder. Compressive stresses were adjusted as required for each composition to produce tablets with nominal SF of 0.69, 0.79, and 0.88. Tablet weights were varied to obtain the intended thicknesses. The punch displacement rate was 5 mm/min for both compression and decompression phases. To allow for any viscoelastic recovery, tablets were stored in airtight scintillation glass vials for at least 24 hours prior to testing for weight, thickness, and breaking force.

Table 1. Monodisperse Granules and Tablets Prepared There From

V-MCC/ V-MNT Particle Size (μm)	Monodisperse Granules				Tablet		
	V-MNT Level (%)	Diameter (mm)	Nominal Thickness (mm)	Nominal Solid Fraction	Nominal Solid Fraction	Nominal Thickness (mm)	Nominal Weight (mg)
200	0	1.5	1.5	0.58	0.69	6	740
	25						850
	50						950
	75				12	1490	
	100					1705	
						1905	

3.4 Characterization

3.4.1 True Density of Powder

The true densities of powder materials were determined from the weight fractions and true densities of individual constituents using Eq. 1 [16]:

$$\rho_{mix} = \frac{(m_1 + m_2 + m_3)}{\left(\frac{m_1}{\rho_1} + \frac{m_2}{\rho_2} + \frac{m_3}{\rho_3}\right)} \quad (1)$$

where m_i and ρ_i denote the weight percent and true density, respectively, of the constituent powder including the lubricant.

3.4.2 Solid Fraction of Monodisperse Granules and Tablets

Monodisperse granule solid fractions and tablet solid fractions were calculated using Eq. 2 [16].

$$SF = \frac{(m/\rho_{mix})}{2 \cdot V_{cup} + A_{die} \cdot (t - 2 \cdot d_{cup})} \quad (2)$$

where m , ρ_{mix} , V_{cup} , A_{die} , t and d_{cup} are defined as compact mass, true density of powder, cup volume of the punch, die hole area, out-of-die thickness of the compact, and cup depth of the punch, respectively. For flat faced tablets V_{cup} and d_{cup} were zero.

3.4.2 Diametrical Tensile Strength of Tablets

Diametrical breaking forces of 6 mm thick tablets were measured using an Instron universal testing machine (model 5569, Instron Ltd. Buckinghamshire, UK) equipped with a 1 kN or a 50 kN load cell. The compression rate was 5 mm/min. Tablet TS (σ_{DC}) was calculated using the following equation [17] :

$$\sigma_{DC} = \frac{2 \cdot F_c}{\pi \cdot D \cdot t} \quad (3)$$

where F_c , D , and t are defined as diametrical breaking force of the compact, diameter of the compact, and out-of-die thickness of the compact, respectively.

The hydrostatic stress (p_{DC}) and the (shear-based) deviatoric stress (q_{DC}) components of the three dimensional stress state were obtained using the following equations [11]:

$$p_{DC} = \frac{2 \cdot \sigma_{DC}}{3} \quad (4)$$

$$q_{DC} = \sqrt{13} \cdot \sigma_{DC} \quad (5)$$

It should be noted that equations 4 and 5 are used for consistency with previous works [10,11,18]. However, the stress state induced by diametrical compression is not uniform throughout the tablet, as discussed by Procopio [19]. Equations 4 and 5 apply only at the center

of the tablet as derived by Cunningham et al. [11]. Both p_{DC} and q_{DC} increase substantially in portions of the tablet closer to the compression platens. Ideally, p_{DC} and q_{DC} would be calculated in the region of the tablet where fracture initiates, but since this region isn't known, equations 4 and 5 are used for consistency.

3.4.3 Uniaxial Compression Strength of Tablets

Uniaxial breaking forces of 12 mm tall tablets were measured using an Instron universal testing machine (model 5569, Instron Ltd. Buckinghamshire, UK) equipped with a 50 kN load cell.

Tablets were compressed axially between two rigid platens at a compression rate of 5 mm/min. To minimize the friction between the platen and the tablet surface, mirror finished platens were lubricated with magnesium stearate powder before each test. Uniaxial compression strength of tablet (σ_{UC}) was calculated using the relation below [11]:

$$\sigma_{UC} = \frac{4 \cdot F_{UC}}{\pi \cdot D^2} \quad (6)$$

where F_{UC} is the uniaxial breaking force. The hydrostatic stress (p_{UC}) and the deviatoric stress (q_{UC}) components of the uniaxial compression stress state were obtained using the following equations [11]:

$$p_{UC} = \frac{\sigma_{UC}}{3} \quad (7)$$

$$q_{UC} = \sigma_{UC} \quad (8)$$

3.4.4 In-die Compaction of Tablets- Axial and Radial Stresses and Elastic Properties

An Instron equipped with a 50 kN load cell, and an instrumented die with 12 mm round flat face punches were used for in-die compaction of 12 mm tall tablets. A piezoelectric stress sensor (2.5 mm diameter, model 6159A- SN4257057, Kistler Instruments AG) was mounted in the die wall, ground cylindrically, and was in contact with the powder compact. The center of the sensor was positioned in the die wall such that it collected radial stress data during compression. The compression and decompression rates were 5 mm/min with zero dwell time. Axial stress data were logged by the Instron data acquisition system. Radial stress data were logged using an Omega OM-SQ2040 data recorder equipped with a Kistler charge amplifier type 5073 - RS232c. Data logging frequency was 100 Hz throughout the compression and decompression processes.

For each compaction cycle, the inner die wall and punch tips were lubricated with magnesium stearate powder prior to adding powder or granules into the die cavity.

The peak axial stress (σ_{ICA}) was calculated as [11]:

$$\sigma_{ICA} = \frac{4 \cdot F_{ICA}}{\pi \cdot D^2} \quad (9)$$

where F_{ICA} is the peak axial force. The peak radial stress (σ_{ICR}) was captured directly by the radial stress sensor.

The hydrostatic stress (p_{IC}) and the deviatoric stress (q_{IC}) components were determined from the maximum axial and radial stresses recorded during the in-die compaction process [11].

$$p_{IC} = \frac{\sigma_{ICA} + 2 \cdot \sigma_{ICR}}{3} \quad (10)$$

$$q_{IC} = \sigma_{ICA} - \sigma_{ICR} \quad (11)$$

The axial strain (ε_A) was calculated using the following equation [11]:

$$\varepsilon_A = \ln[(H_0 - P_U + P_D)/H_0] \quad (12)$$

where H_0 is the initial specimen height, P_U is the upper punch displacement, and P_D is the punch deformation determined by compressing the punches in an empty die cavity.

From the slope of the decompression phase of the axial and radial stress versus axial strain profiles, Poisson's ratio (ν) and Young's modulus (E) were calculated using Eqs. 13 and 14 [11]. A linear fit of the first 200 data points of the decompression phase (two seconds) was used to calculate slopes for all the samples. Assumptions are made that the radial strain is zero, and the circumferential and radial stresses are equal.

$$\nu = \frac{\left(\frac{d\sigma_{ICR}}{d\varepsilon_A^e}\right)}{\left(\frac{d\sigma_{ICR}}{d\varepsilon_A^e}\right) + \left(\frac{d\sigma_{ICA}}{d\varepsilon_A^e}\right)} \quad (13)$$

$$E = \left(\frac{d\sigma_{ICA}}{d\varepsilon_A^e}\right) - 2\nu \cdot \left(\frac{d\sigma_{ICR}}{d\varepsilon_A^e}\right) \quad (14)$$

where $\left(\frac{d\sigma_{ICA}}{d\varepsilon_A^e}\right)$ and $\left(\frac{d\sigma_{ICR}}{d\varepsilon_A^e}\right)$ are the slopes of the axial and radial stress versus axial strain profile, respectively, of the decompression phase.

3.4.5 Determination of DPC Parameters

DPC parameters as defined in Figure 1 were determined at each tablet SF, based on the work by Cunningham et al. [11] from the uniaxial compression test, diametrical breaking force test, and in-die compression axial and radial strain data. cohesion (d) of the material was calculated using the following equation:

$$d = \frac{\sigma_{UC} \cdot \sigma_{DC} \cdot (\sqrt{13} - 2)}{\sigma_{UC} + 2 \cdot \sigma_{DC}} \quad (15)$$

The internal friction angle (β) of the material was calculated using Eq. 16:

$$\beta = \tan^{-1} \left[\frac{3 \cdot (\sigma_{UC} - d)}{\sigma_{UC}} \right] \quad (16)$$

The pressure evolution parameter (p_a) was calculated using the following equation:

$$p_a = \frac{-(3 \cdot q_{IC} + 4 \cdot d \cdot \tan\beta) + \sqrt{(9 \cdot q_{IC}^2 + 24 \cdot d \cdot q_{IC} \cdot \tan\beta + 24 \cdot p_{IC} \cdot q_{IC} \cdot (\tan\beta)^2 + 16 \cdot q_{IC}^2 \cdot (\tan\beta)^2)}}{4 \cdot (\tan\beta)^2} \quad (17)$$

The cap eccentricity parameter (R) was calculated using Eq. 18:

$$R = \sqrt{\frac{2 \cdot (p_{IC} - p_a)}{3 \cdot q_{IC}}} \quad (18)$$

The hydrostatic yield strength (p_b) of the material was calculated using the following equation:

$$p_b = p_a + R \cdot [d + p_a \cdot \tan\beta] \quad (19)$$

3.4.5 Imaging of Monodisperse Granules and Tablets

Scanning electron microscopic (SEM) images of monodisperse granules were taken with an FEI Quanta 200 FEG SEM (version 2.4, FEI Company, OR, USA). Samples were coated with gold:paladium (60:40) and scanning was completed at 0.3 Torr pressure and 10 kV beam energy.

Optical images of tablets of all compositions and SF were collected using a Keyence digital microscope.

4. Results and Discussion

4.1 Monodisperse Granules

SEM images of monodisperse granules of each composition are shown in Figure 3. With increasing MNT concentration, a more bi-disperse particle size distribution on the granule surface is visible suggestive of attrition of a more brittle material. In comparison, the MCC granules appear to be more plastically deformable.

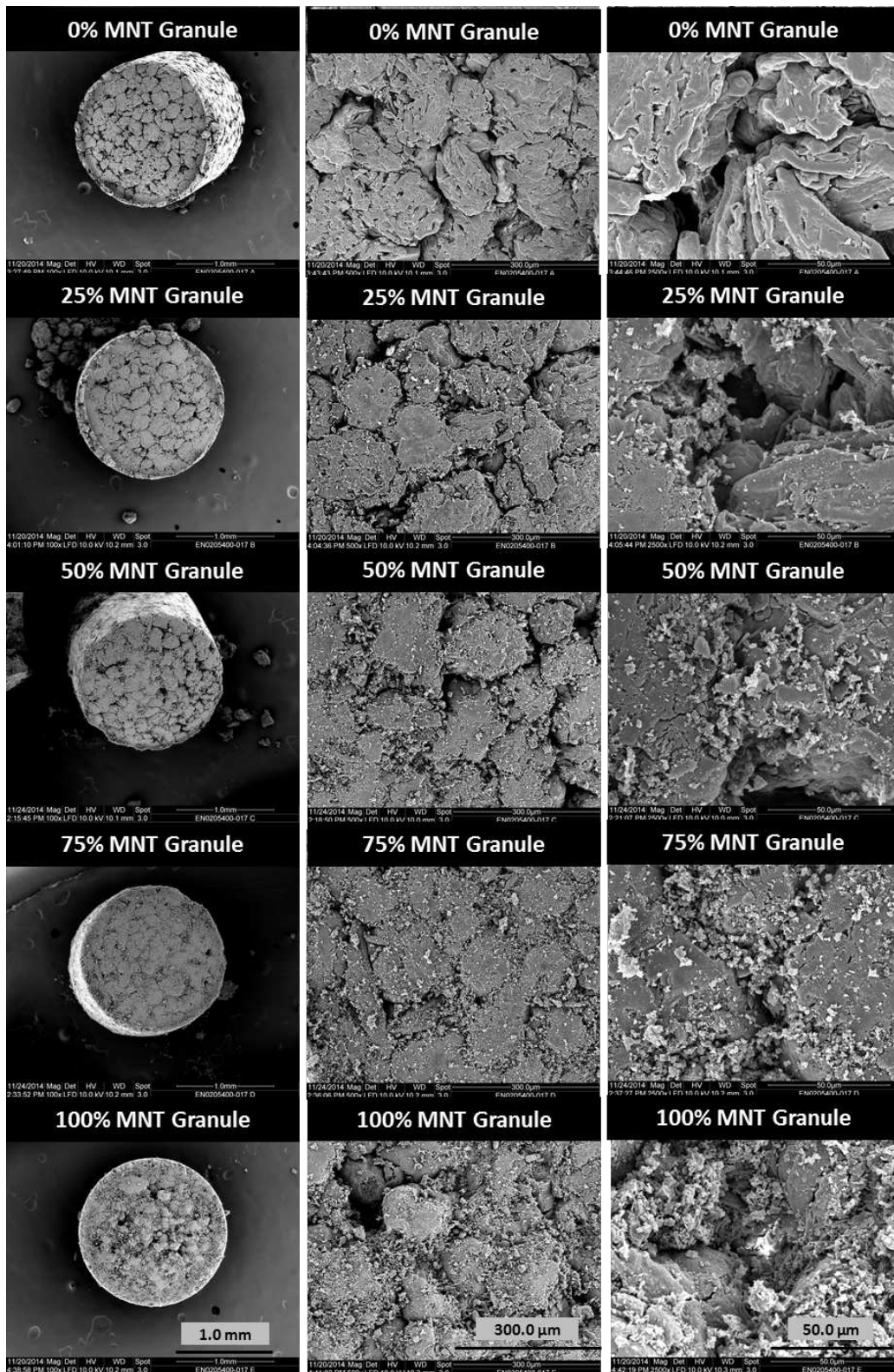


Figure 3. SEM Images of Monodisperse Granules. MNT level increases top to bottom. Magnification increases left to right.

3.4 Tablets Produced from Monodisperse Granules

Figure 4 shows optical images of tablets at each composition and SF. There was a substantial difference in the tablet matrix depending upon the granule composition and tablet SF. Granules boundaries were clearly visible in tablets prepared from MCC granules even in the 0.88 SF tablet. The appearance of residual grain structure suggests that granules plastically deformed during tablet compression, extruding into the pore spaces between granules. With increasing MNT level, tablet surfaces became smoother, suggestive of a more monolithic tablet. The tablet appearance suggests that MNT granules likely fractured during compression and completely filled the pore space between granules.

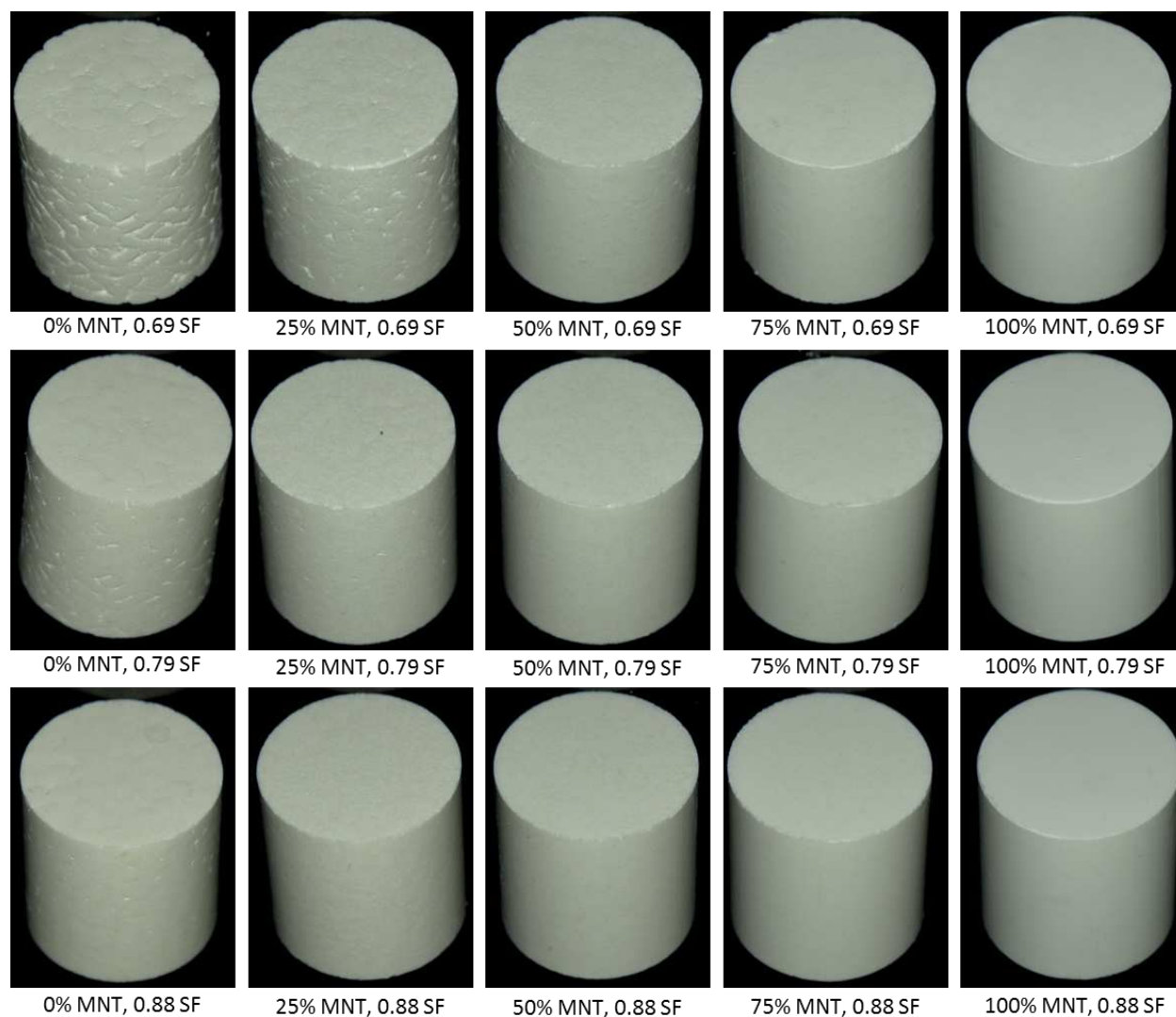


Figure 4. Optical Images of 12 mm Tall Tablets Prepared from Monodisperse Granules. MNT level increases left to right. Tablet SF increases top to bottom.

The peak axial stress exerted by the upper punch and the peak radial stress transmitted to the die wall during the confined compression process are plotted against the granule composition in Figure 5 and Figure 6, respectively. For 0.69 SF tablets, both the axial and radial stresses decreased slightly as the MNT level in the granule increased. However, the trend was reversed for higher tablet SF. Axial and radial stresses increased slightly at a 0.79 tablet SF, but substantially at a 0.88 tablet SF. At low tablet SF, the secondary structure of the agglomerated spray dried MNT particles likely collapsed easily (Figure 2). In general, irrespective of the granule composition, the radial stresses were approximately 30%, 39% and 48% of the axial stress for 0.69, 0.79 and 0.88 SF tablets, respectively.

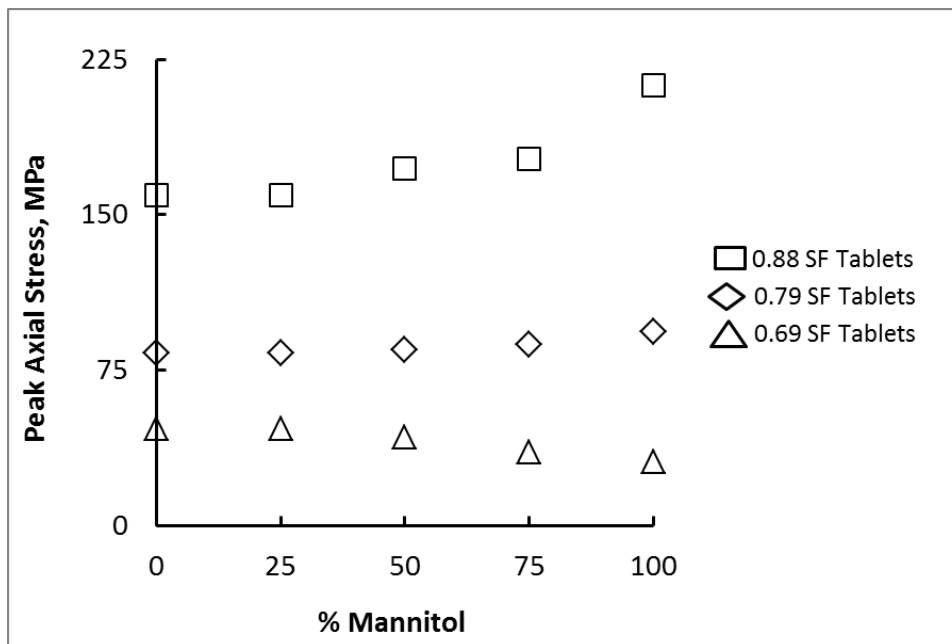


Figure 5. Axial Stress versus MNT level in the Granule. Triangle (Δ), diamond (\diamond) and square (\square) markers represent nominally 0.69, 0.79, and 0.88 SF tablets, respectively.

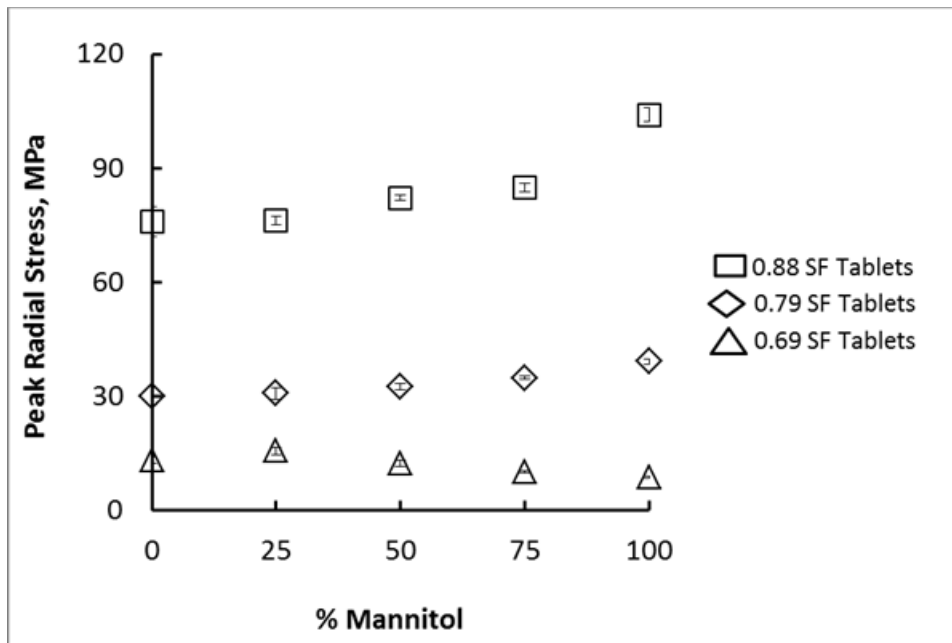


Figure 6. Radial Stress versus MNT level in the Granule. Triangle (Δ), diamond (\diamond) and square (\square) markers represent nominally 0.69, 0.79, and 0.88 SF tablets, respectively.

In Figure 7, shows optical images of diametrically fractured tablets of 0.88 SF. Here again, images suggest a more ductile nature of MCC (0% MNT) granules compared with 100% MNT granules. For the MCC-rich tablets, the fracture plane does not appear to completely cleave the tablets. Fracture planes also appear to bifurcate close to the platens, suggestive of locally high shear stresses and potentially tablet flattening near the compression platen [19,20]. In comparison, the 75% MNT tablets failed with a linear fracture line, suggestive of classic brittle fracture. Interestingly, the pure MNT tablets exhibited triple cleft fracture which is reported in the literature as tensile failure [20, 21]. This observation qualitatively suggests the transition of tablets from ductile to brittle nature as the MNT level in the granule increases.

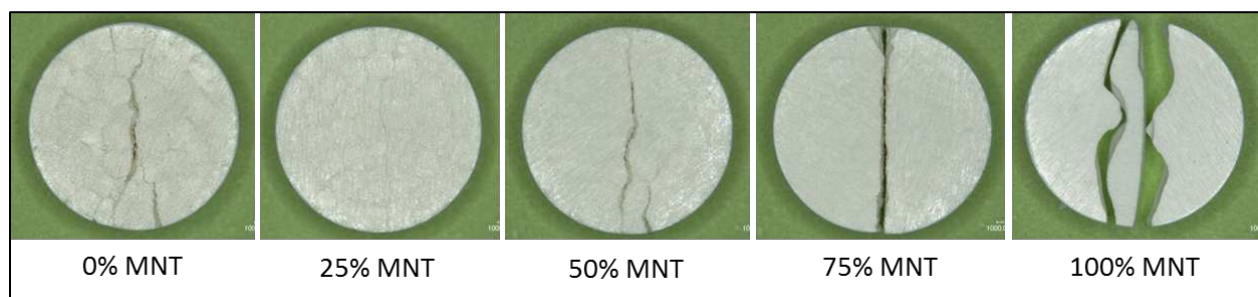


Figure 7. Optical Image of Diametrically Fractured Tablets (0.88 SF). MNT level increases left to right.

Diametrical TS of tablets of nominally 0.69, 0.79, and 0.88 SF are plotted against MNT level in Figure 8. TS of 0.69 SF tablets decreased slightly as the MNT level increased. However, as the tablet SF increased, a non-linear relationship was apparent with a maximum near 75% MNT. The TS of 0.88 SF tablets prepared from the 75% MNT granules was the highest, followed by the 50% MNT granules. Surprisingly, the TS of tablets prepared from MCC granules was either similar to or slightly lower than the MNT granules. Another complicating factor in the analysis of data in Figure 8 is that only the 75% MNT tablets fractured along the centerline for which the calculation of tensile strength by Eq. 3 is applicable. Fracture in the other tablets may have originated close to the compression platens where the stress states (and therefore the actual tablet strengths) may have been larger than predicted by Eq. 3.

Figure 9 shows plots of uniaxial compression strength versus granule composition. Tablets prepared from MCC granules possessed the highest uniaxial strength. Strength decreased monotonically as the MNT level in granules increased. Compared to the MCC tablets, 50% and 75% MNT tablets have higher diametrical TS but lower uniaxial compressive strength.

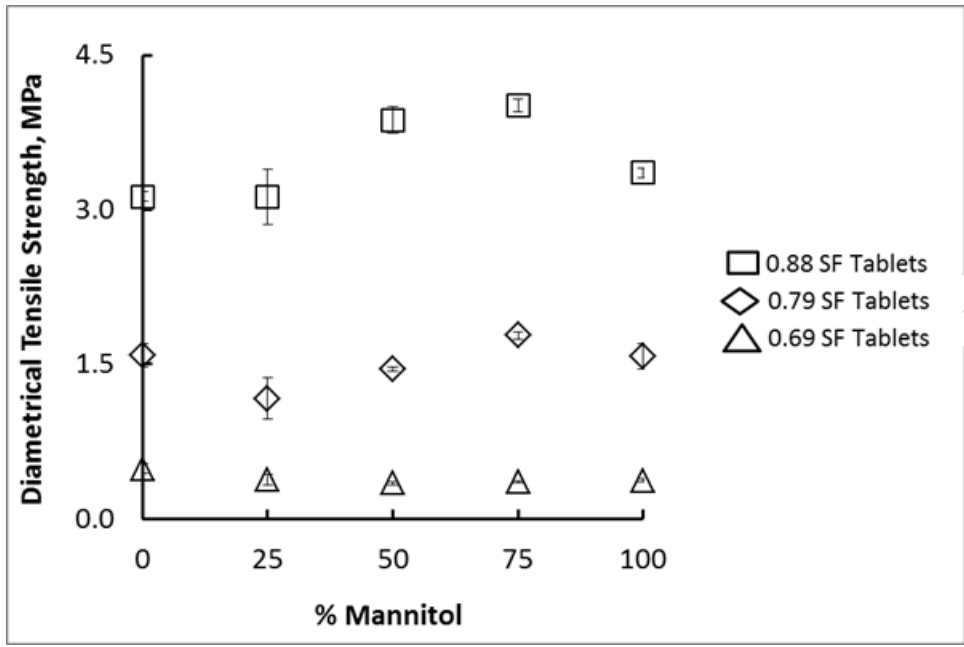


Figure 8. Diametrical Tensile Strength of Tablets (6 mm tall) versus MNT Level in the Granule. Triangle (Δ), diamond (\diamond) and square (\square) markers represent nominally 0.69, 0.79 and 0.88 SF tablets, respectively.

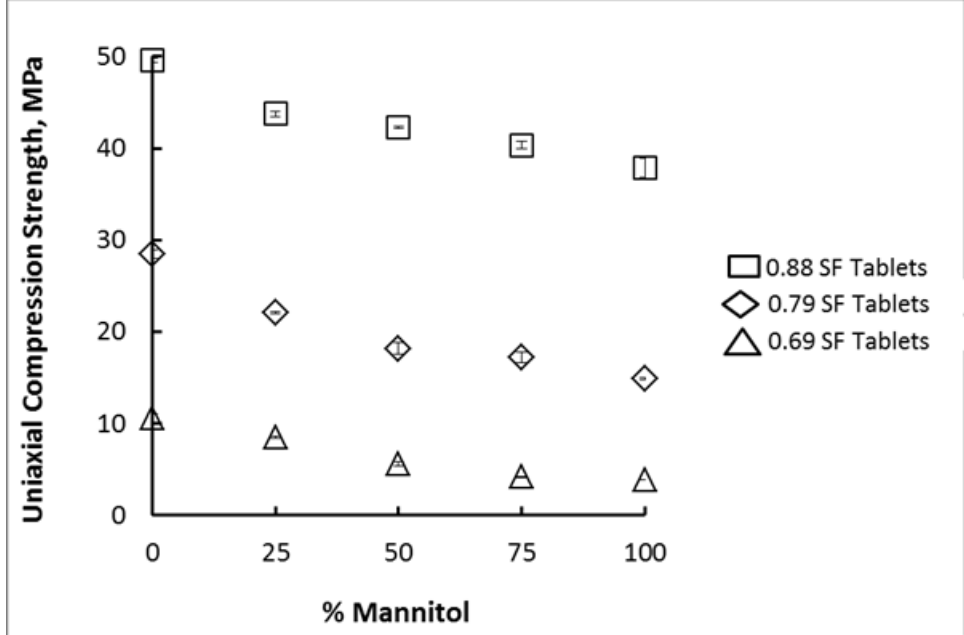


Figure 9. Uniaxial Compression Strength of Tablets (12 mm tall) versus MNT Level in the Granule. Triangle (Δ), diamond (\diamond) and square (\square) markers represent nominally 0.69, 0.79, and 0.88 SF tablets, respectively.

3.5 DPC Parameters

In Figure 10, cohesion (d) of materials is plotted against MNT level in granules. The plots showed a trend that is comparable to what was seen for diametrical TS of tablets (Figure 8), as expected since d is calculated from the diametrical tensile strength data. At 0.79 and 0.88 tablet SF, d and granule composition exhibited a non-linear relationship. At 0.88 tablet SF, 75% MNT granules have a 25% higher cohesion than pure MCC tablets and 20% higher cohesion than pure MNT tablets. At 0.88 tablet SF, d is the highest (8 MPa) for 75% MNT granules which is only slightly higher (7.8 MPa) than 50% MNT granules. Although a trend for 0.69 tablet SF is not obvious in Figure 10 due to the large Y-scale compared to the data points, a similar trend is present. The cohesion of MCC granules was similar to, or slightly lower than, MNT granules.

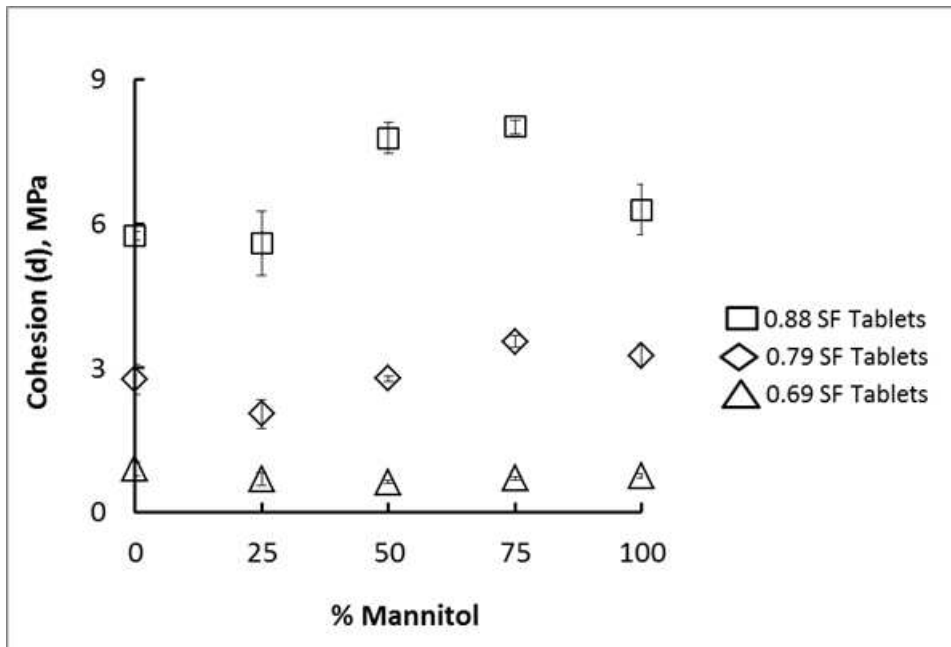


Figure 10. Cohesion versus MNT Level in Granules. Triangle (Δ), diamond (\diamond) and Square (\square) markers represent nominally 0.69, 0.79, and 0.88 SF tablets, respectively.

Figure 11 shows internal angle of friction (β) against MNT level in the tablets. β was only slightly impacted by granule composition or tablet SF. There was a trend of slightly lower β as the MNT level increased. However, the range of β was very small, varying between 67° and 70° . Such a small difference in β of granules will have only little impact on susceptibility of tablets to failure.

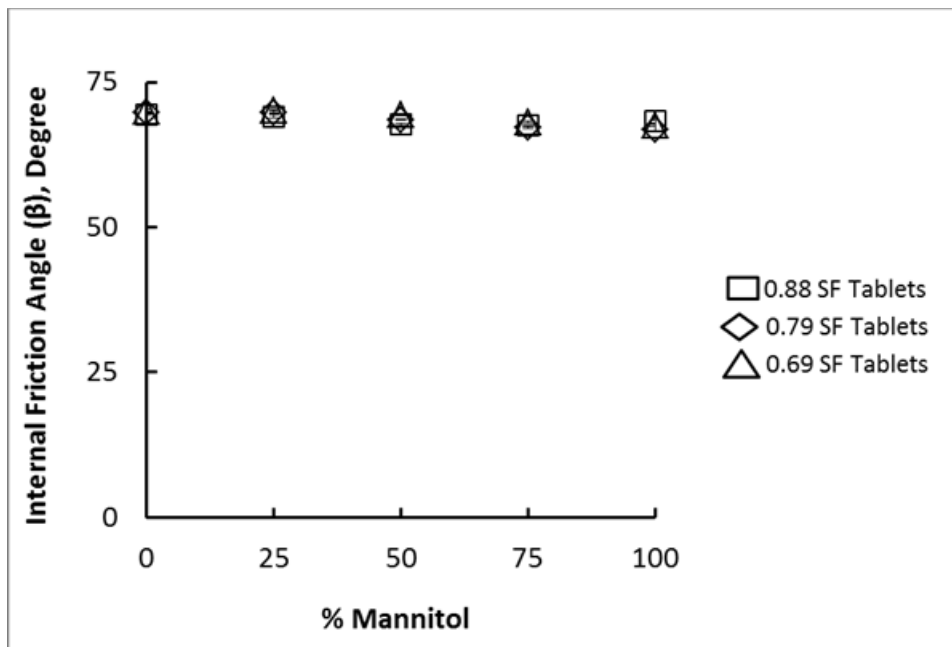


Figure 11. Internal Friction Angle versus MNT level in Granules. Triangle (Δ), diamond (\diamond) and square (\square) markers represent nominally 0.69, 0.79, and 0.88 SF tablets, respectively.

Figure 12 plots the hydrostatic stress at the onset of evolution of cap (cap evolution parameters, P_a) against MNT level in granules for 0.69, 0.79 and 0.88 SF tablets. P_a for 0.69 SF tablets was slightly smaller as the MNT level in the granules increased. However, P_a was larger for 0.79 and 0.88 SF tablets as the as the MNT level increased and the rate of increase was higher at 0.88 tablet SF. P_a for MNT granules was $\sim 33\%$ higher than the MCC granules at 0.88 SF. This could be attributed to densification of spray dried MNT particles by collapsing the porous agglomerated structure at low SF and then fracture of the mannitol crystals at high SF (Figure 2).

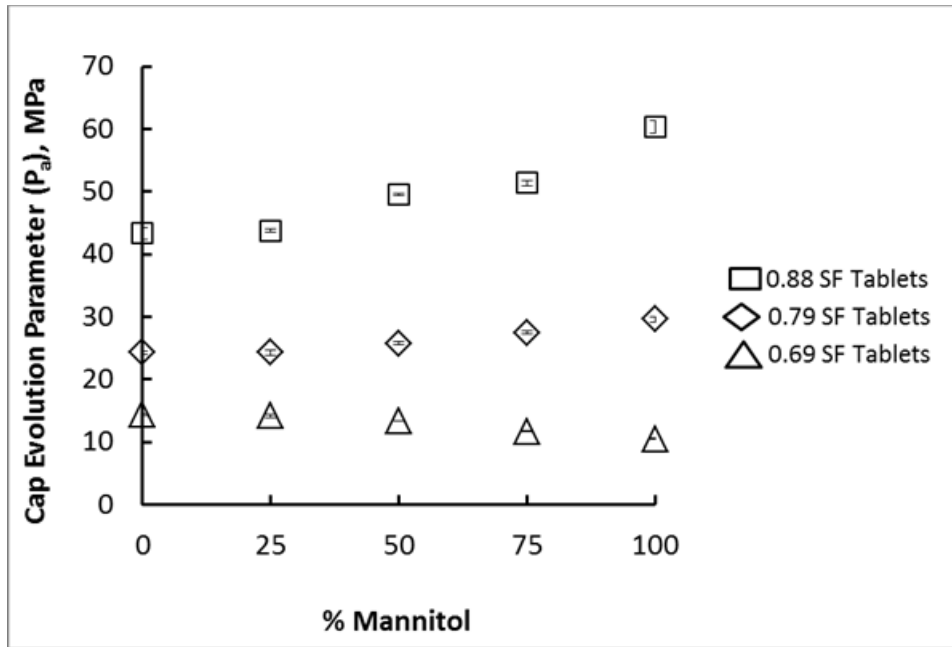


Figure 12. Cap Evolution Parameter versus MNT level in Granules. Triangle (Δ), diamond (\diamond) and Square (\square) markers represent nominally 0.69, 0.79, and 0.88 SF tablets, respectively.

Figure 13 shows the cap eccentricity parameters (R) against the MNT level in granules. The R value was 0.44, 0.56 and 0.69 for nominally 0.69, 0.79 and 0.88 SF tablets, respectively. Cap eccentricity was not significantly impacted by the granule composition. As the MNT level increased, R decreased slightly at 0.69 tablet SF; however, R increased slightly at 0.79 and 0.88 tablet SF. Once the tablet SF reaches 1, the tablet would not densify any further even at a very high applied stress (fully dense material behavior) [18]. However, the compact would have elastic properties and could fail by fracture.

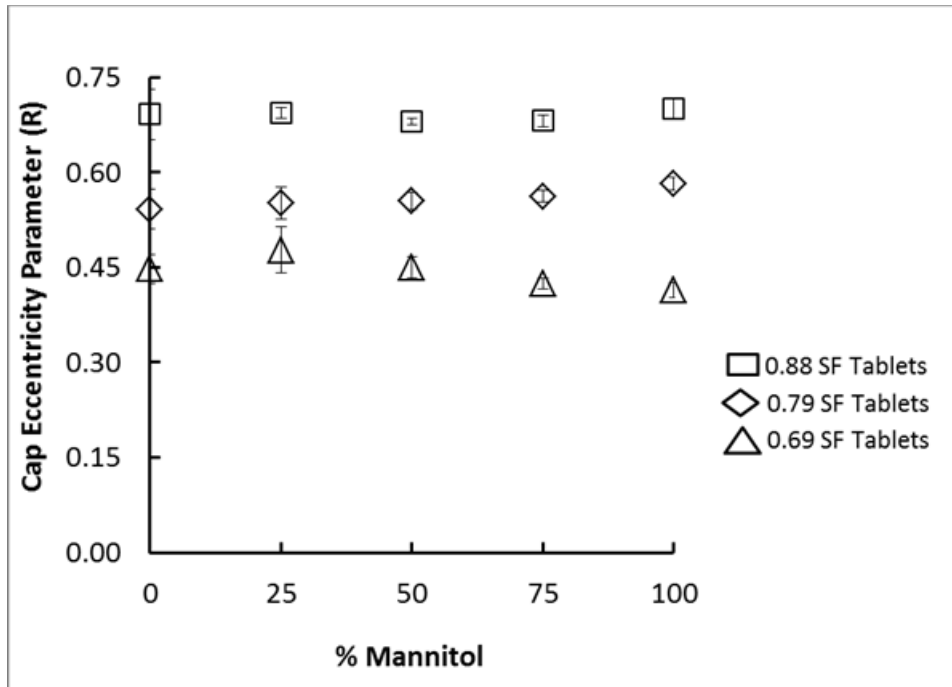


Figure 13. Cap Eccentricity Parameter versus MNT level in Granules. Triangle (Δ), diamond (\diamond) and Square (\square) markers represent nominally 0.69, 0.79, and 0.88 SF tablets, respectively.

Figure 14 plots the hydrostatic yield strength (P_b) of materials against the MNT level in granules. The data follow a trend similar to the cap evolution parameter (Figure 12). P_b was significantly impacted by the MNT level in granules and the tablet SF. P_b slightly decreased with increasing MNT level in the granules for 0.69 SF tablets; it was ~34% lower for MNT granules than MCC granules. However, the trend was reversed for higher tablet SF. P_b increased with the MNT level in granules for 0.79 and 0.88 SF tablets, and the rate of increase was higher at 0.88 tablet SF. Compared to MCC granules, P_b for MNT granules was ~14% and ~40% higher at 0.79 and 0.88 tablet SF, respectively. Thus the amount of stress required to further densify the compact depends on the granule composition.

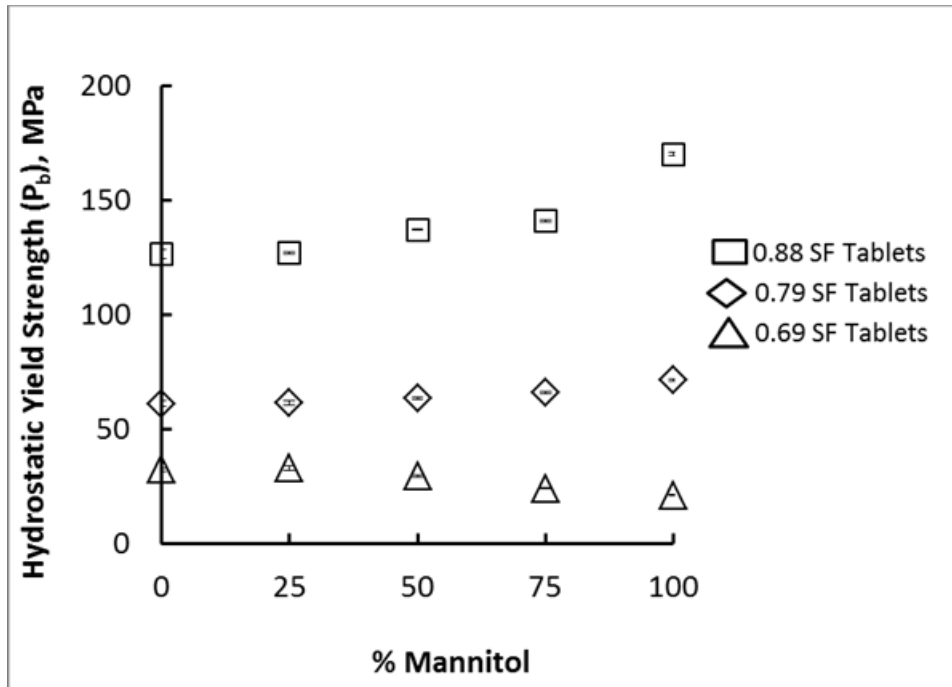


Figure 14. Hydrostatic Yield Stress versus MNT level in granules. Triangle (Δ), diamond (\diamond) and Square (\square) markers represent nominally 0.69, 0.79, and 0.89 SF tablets, respectively.

In Figure 15, shows the DPC model fitting curves in the p - q plane for 0.69 SF, 0.79 SF and 0.88 SF tablets prepared from pure MCC granules, MCC/MNT binary granules, and pure MNT granules. The p and q components of the diametrical tensile stress (open markers), uniaxial compression stress (grey markers), and maximum in-die compaction stress (black markers) at each SF are also shown in the plot. The granule composition, 0, 25, 50, 75, and 100% MNT are represented by the symbols square (\square), diamond (\diamond), triangle (Δ), circle (O), and star (*), respectively. Although four independent variables are required to calibrate the DPC model, there are only three data points per DPC envelope. The fourth parameter to satisfy the requirement is the normality of the plastic flow vector (associative flow rule) [11,22,23].

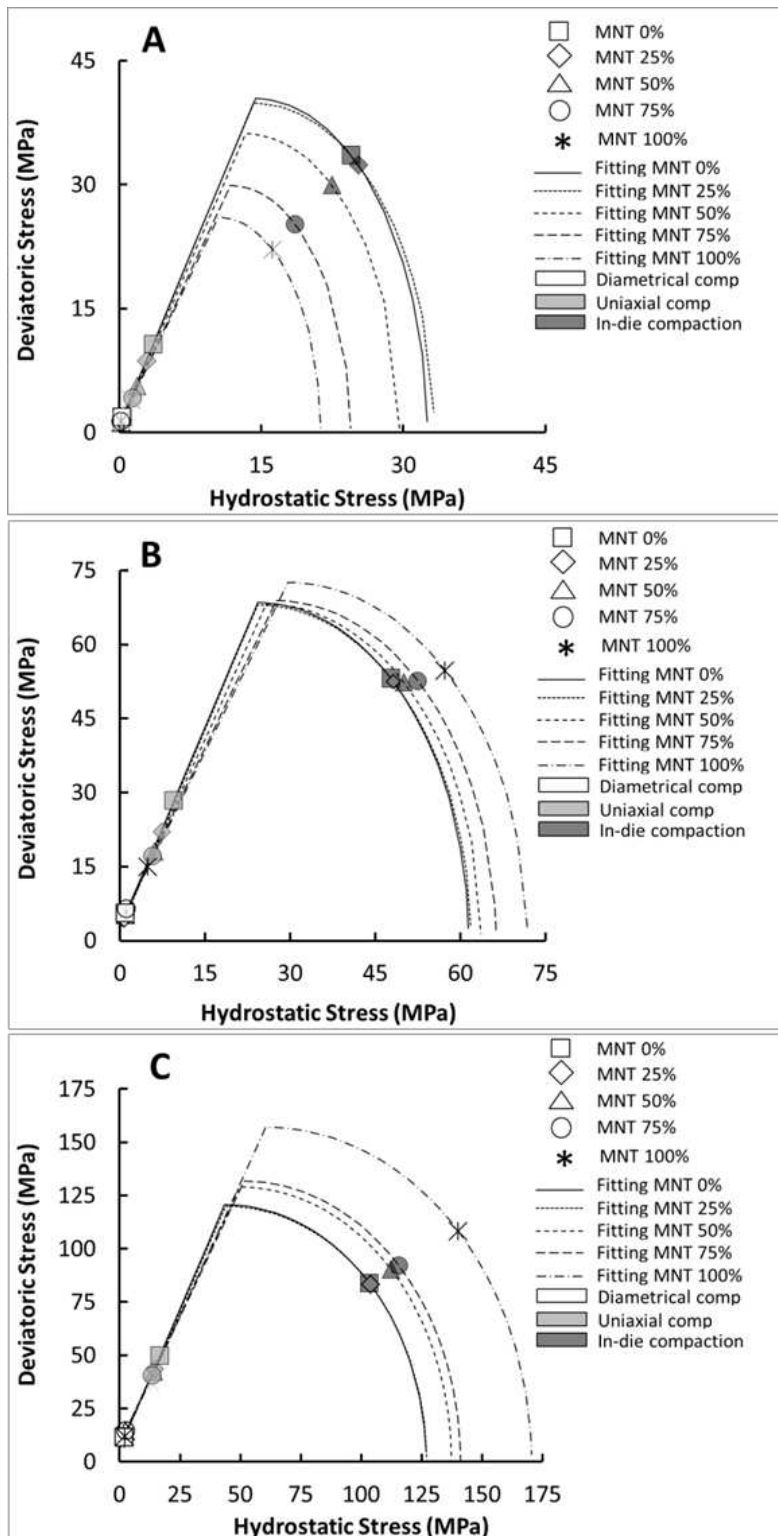


Figure 15. DPC Profiles for MCC Granules, MCC/MNT Binary Granules, and MNT Granules at A) 0.69, B) 0.79, and C) 0.89 Tablet Solid Fraction.

The plots in Figure 15 clearly show that the yield surfaces for pure MCC and 25% MNT granules are comparable but that for granules with 50% or higher level of MNT are significantly different. At 0.69 tablet SF, the yield locus contracts as the MNT level in granules increases to 50% or higher. At this SF, tablets prepared from pure MNT granules have the smallest yield surface and the largest for pure MCC and 25% MNT granules. However, the trend reverses as the tablet SF increases. At 0.79 and 0.88 tablet SF, the pure MCC and 25% MNT granules have the smallest yield surface and the pure MNT granules have the largest surface, with larger expansions at 0.88 tablet SF. Possibly, the two stage deformation of spray dried MNT particles causes this shift in yield surface-- the porous agglomerates of MNT may collapse under a low stress whereas, fracturing the primary MNT crystals may require high stress (Figure 2). At the onset of densification, the hydrostatic to deviatoric stress ratio is similar, ~ 0.38 for all tablet SF. However, the p to q ratio of the maximum in-die compaction stress on the stress path increases significantly from ~ 0.75 at 0.69 tablet SF to ~ 0.86 at 0.79 tablet SF and ~ 1.26 at 0.88 tablet SF.

In Figures 16 and 17, Poisson's ratios and Young's moduli, respectively, are plotted against MNT level. Poisson's ratio increased with increasing tablet SF, and with decreasing MNT concentration. Larger increases were observed at higher tablet SF. In contrast, Poisson's ratio for MNT granules was insensitive to the tablet SF. Young's moduli were not significantly affected by the granule composition at 0.69 tablet SF. However, at 0.79 and 0.88 tablet SF, Young's modulus increased with increasing MNT level with a significantly higher rate of increase at 0.88 tablet SF.

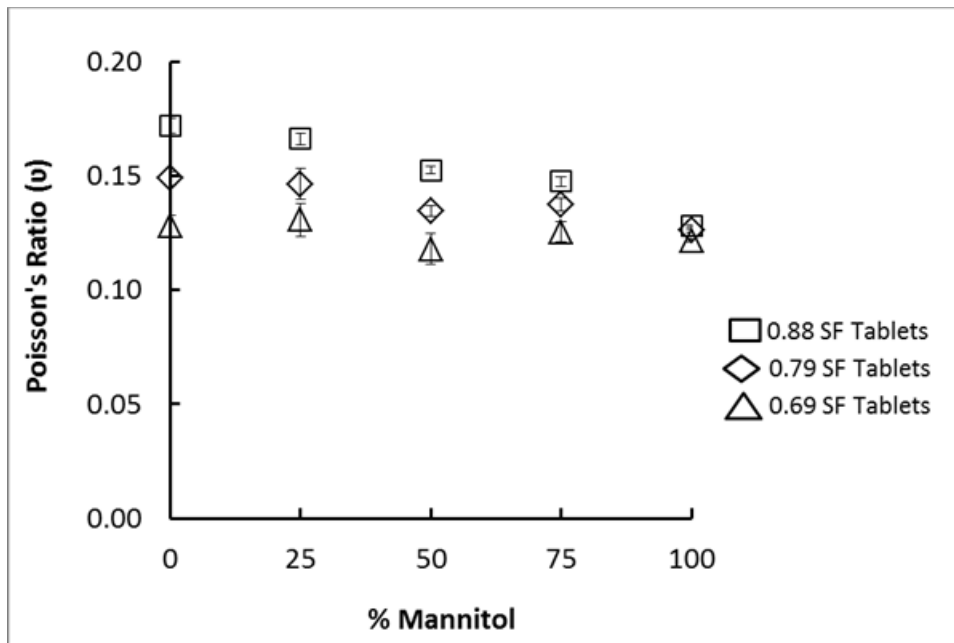


Figure 16. Poisson's Ratio versus MNT Level in Granules. Triangle (Δ), diamond (\diamond) and square (\square) markers represent nominally 0.69, 0.79, and 0.89 SF tablets, respectively.

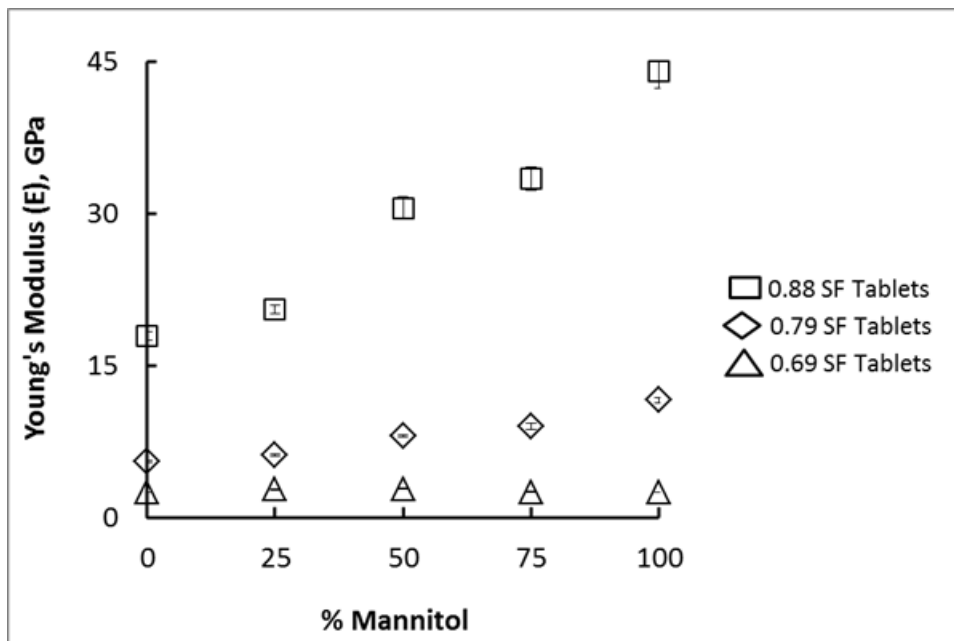


Figure 17. Young's Modulus versus Granule Solid Fraction. Triangle (Δ), diamond (\diamond) and square (\square) markers represent nominally 0.69, 0.79, and 0.89 SF tablets, respectively.

5. Discussion

Calibration of DPC parameters in this study allows understanding the effect of granule composition on the compaction properties of deformable granules independent of their SF. The ratio of MCC to MNT in dry granules affects the compaction properties of granules and the fracture and elastic behavior of the tablets. Higher level of MNT in granules requires a lower compression pressure to obtain a low SF tablet but higher compression pressure to obtain a high SF tablets. This is illustrated by the contraction or expansion of the cap surface with associated change in cap evolution parameter, cap eccentricity parameter, and hydrostatic yield stress depending upon the granule composition and tablet SF. The shear failure line is slightly impacted by the granule composition, which could be considered reasonable based on the small difference (1 MPa or less) between the minimum and maximum TS of tablets. Both the diametrical TS of tablets and the cohesion of tablets follow the same trend. 75% MNT in the formulation has the highest cohesion and diametrical TS at a pharmaceutically relevant tablet SF of 0.88. Tablets prepared from high MNT level are stiffer with smaller Poisson's ratio and would experience lower relaxation during the unloading and ejection step.

The effect of granule composition on all the compaction properties of granules does not follow the simple linear mixing rule proposed by Kuentz et al. [24]. Table 2 shows the summary of the applicability of the linear mixing rule to various properties measured in this study. The maximum % error of the linear mixing rule is shown in the parenthesis. For some properties such as uniaxial compression strength, hydrostatic yield strength, young's modulus, Poisson's ratio, linear rules are not perfect, but close where some interaction between the constituents are present. These properties change monotonically with the composition. Some property is just insensitive to composition (e.g., internal angle of friction). On the other hand, for properties such

as cohesion and diametrical TS, the linear mixing rule is clearly inappropriate. These properties go through a maximum as %MNT increases in the formulation. This is consistent with direct compression of MCC/spray dried lactose binary mixture, for which the crushing strength of tablets goes through a maximum at 50%/50% composition [25]. The implication of this finding is that many of the compaction properties of binary mixtures of MCC/MNT may be estimated to a reasonable approximation from the properties of individual component using the linear mixing rule. However, the most frequently measured mechanical property, the TS of MCC/MNT tablets may not be reasonably estimated from the TS of pure MCC and pure MNT tablets using the linear mixing rule.

Table 2. Applicability of the Linear Mixing Rules to the Compaction Properties of MCC/MNT Binary Granules

Parameters/Properties	Apparent applicability of the Linear Mixing Rule	Approximate Trend at Tablet SF (Maximum % Error of Prediction)		
		0.69	0.79	0.88
Axial stress	Approximately linear	-- (-9.3%)	-- (4.0%)	↑ (11.1)
Radial stress	Approximately linear	-- (-28.4%)	-- (5.9%)	↑ (12.5%)
Uniaxial compression strength	Approximately linear	↓ (25.0%)	↓ (16.2%)	↓ (6.2%)
Diametrical TS	Not linear, maximum at 75% MNT	Sigmoid (19.1%)	Sigmoid (26.4%)	Sigmoid (-21.5%)
Cohesion (d)	Not linear, maximum at 75% MNT	Sigmoid (23.9%)	Sigmoid (29.2%)	Sigmoid (-30.1%)
Cap evolution parameter (P_a)	Approximately linear	↓ (-7.5%)	↑ (5.3%)	↑ (8.4%)
Hydrostatic yield strength (P_b)	Approximately linear	↓ (-11.8%)	↑ (4.4%)	↑ (11.5%)
Cap eccentricity parameter (R)	Not sensitive	↓ (-8.85%)	↑ (1.7%)	-- (2.5%)
Internal friction angle (β)	Not sensitive	-- (-1.0%)	-- (-1.2%)	-- (1.5%)
Young's modulus (E)	Approximately linear	↓ (-13.8%)	↑ (12.2%)	↑ (16.1%)
Poisson's ratio (ν)	Approximately linear	↓ (5.4%)	↑ (-4.3%)	↑ (-6.0%)

(↓) Monotonically decreases as MNT level increases

(↑) Monotonically increases as MNT level increases

(--) Little or no interaction

6. Conclusions

Calibration of the DPC model using monodisperse granules of MCC/MNT binary mixtures determined the effect of the composition on the compaction properties of dry granules without the interference from the effect of granule SF. Higher level of MNT in granules required a lower compression pressure to obtain a low SF tablet but higher compression pressure to obtain a high SF tablets. At an industrially relevant tablet SF of 0.88, 75% MNT granules exhibited the highest cohesion, and produced the strongest tablets. The Young's modulus increased and the Poisson's ratio decreased with increasing level of MNT in the composition.

The effect of granule composition on all the compaction properties of granules does not follow a simple linear mixing rule. Properties such as cohesion and diametrical TS go through a maximum as %MNT increases in the formulation and clearly do not follow the linear mixing rule. On the other hand, properties such as hydrostatic yield strength, young's modulus, Poisson's ratio approximately follow the linear mixing rule, where some interactions between the constituents are present. Some properties (e.g., internal angle of friction) are just insensitive to the composition. The compaction properties of dry granules of a multicomponent system may not be precisely estimated from the properties of individual components, simply by using the linear mixing rule.

References

- [1] J. Litster, B. J. Ennis, *The science and engineering of granulation processes*, Kluwer Academic Publishers, 2004.
- [2] B. Mitra, J. Hilden, J. D. Litster, Novel use of monodisperse granules to deconvolute impacts of granule size versus granule solid fraction on tablet tensile strength, *Advanced Powder Technology*, 26 (2015) 553-562
- [3] B. Mitra, J. Hilden, J. D. Litster, **Color granules**, *Powder Technology* (submitted), 2015
- [4] B. Mitra, J. Hilden, J. D. Litster, Compaction mechanics of plastically deformable dry granules, *Powder Technology* (submitted), 2015
- [5] S. Inghelbrecht, J. P. Remon, Roller compaction and tableting of microcrystalline cellulose/drug mixtures. *Int J Pharm.* 161 (1998) 215-224
- [6] A. Gupta, G. E. Peck, R. W. Miller, K. R. Mosis, Real time NIR monitoring of CU, moisture content, compact density, TS and and Young's modulus of roller compacted powder blends. *J. Pharm. Sci.*, 94 (2005) 1589-1597
- [7] E. Hadzovic, G. Betz, S. Hadzidedic, S. K. El-Arini, H. Leuenberger, Investigation of compressibility and compactibility parameters of roll compacted theophylline and its binary mixtures. *Int. J. Pharm.*, 416 (2011) 97-103
- [8] M. G. Herting, P. Kleinbudde, Roll compaction/dry granulation: effect of raw material particle size on granule and tablet properties. *Int. J. Pharm.* 338 (2007) 110-118
- [9] L. Farber, K. P. Hapgood, J. N. Michaels, X. Y. Fu, R. Meyer, M. A. Johnson, Unified compaction curve model for TS of tablets made by roll compaction and direct compression. *Int. J. Pharm.*, 346 (2008) 17-24.
- [10] K. LaMarche, D. Buckley, R. Hartley, F. Qian, S. Badawy, Assessing materials' tablet compaction properties using the Drucker-Prager Cap model, *Powder Technology*, 267 (2014) 208-220
- [11] J. Cunningham, I.C. Sinka, A. Zavalings, Analysis of tablet compaction. I. Characterization of mechanical behavior of powder and powder/tooling friction. *J Pharm Sci.*, 93 (2004) 2022-2039
- [12] Katharina M Picker-Freyer, An insight into the process of tablet formation of microcrystalline cellulose. *J. of Thermal Analysis and Calorimetry*, 89 (2007) 745-748.
- [13] W. L. Hulse, R. T. Forbes, M. C. Bonner, M. Getrost, The characterization and comparison of spray-dried mannitol samples Characterization of spray-dried mannitol, *Drug Development and Industrial Pharmacy*, 35 (2009) 712-718

-
- [14] C. C. Sun, Mechanism of moisture induced variations in true density and compaction properties of microcrystalline cellulose, *International Journal of Pharmaceutics*, 346 (2008) 93-101
- [15] R. C. Rowe, P. J. Seskey, S. C. Owen, eds, *Handbook of Pharmaceutical Excipients*, 7th edition, London, Pharmaceutical Press, 2012, pp 479-482
- 16] J. Hilden, G. Earle, Prediction of roll compacted ribbon solid fraction for quality by design development, *Powder Technology*, 213 (2011) 1–13.
- [17] J. T. Fell and J. M. Newton, 1970, Determination of tablet strength by the diametrical compression test, *J. Pharm. Sci.*, 59 (1970), 688-691
- [18] I.C. Sinka, J. Cunningham, A. Zavaliangos, 2003. The effect of wall friction in the compaction of pharmaceutical tablets with curved faces: a validation study of the Drucker-Prager Cap model, *Powder Technol*, 133 (2003) 33-43
- [19] A. Procopio, A. Zavaliangos, J. Cunningham, 2003, Analysis of the diametrical compression test and the applicability to plastically deforming materials, *J. Mat. Sci.*, 38 (2003) 3629 – 3639
- [20] G. Alderborn, Particle, Tablets and Compaction, in: M. Aulton, K. Taylor (Eds), *Aulton's Pharmaceutics: The Design and Manufacture of Medicines*, 4th edition, Elsevier Ltd., London, 2013, pp 530-550
- [21] A. Rudnick, A.R. Hunter, F.C. Holden, An Analysis of the Diametrical Compression Test, *Mater. Res. Stand.*, 3 (1963) 283-289
- 22 H. Diarra, V. Mazel, A. Boillon, L. Rehault, V. Busignies, S. Bureau, P. Tchoreloff, Finite element method (FEM) modeling of the powder compaction of cosmetic products: comparison between simulated and experimental results, *Powder Technology*, 224 (2012) 233-240
- [23] W. F. Chen, D. J. Han, Stress strain relations for perfectly plastic materials, In: *Plasticity for Structural Engineers*, 2007, J Ross Publishing, Fort Lauderdale, FL
- [24] M. Kuentz, H. Leuenberger, A new theoretical approach to tablet strength of a binary mixture consisting of a well and a poorly compactable substance, *Eur. J. Pharm. Biopharm.*, 49 (2000) 151-159
- [25] H. Vromans, C. F. Lerk, Densification properties and compactibility of mixtures of pharmaceutical excipients with and without magnesium stearate. *Int. J. Pharm.* 46 (1988) 183-192